

Non-Equilibrium Phase Transition in an Atomistic Glassformer: the Connection to Thermodynamics

Francesco Turci,^{1, 2} C. Patrick Royall,^{1, 2, 3} and Thomas Speck⁴

¹*H.H. Wills Physics Laboratory, University of Bristol, Bristol, BS8 1TL, UK*

²*Centre for Nanoscience and Quantum Information, Bristol BS8 1FD, UK*

³*School of Chemistry, University of Bristol, Bristol BS8 1TS, UK*

⁴*Institut für Physik, Johannes Gutenberg-Universität Mainz, Staudingerweg 7-9, 55128 Mainz, Germany*

The physics underlying the glass transition is a major outstanding problem in condensed matter. Central to resolving this problem is whether there is some kind of thermodynamic transition to an “ideal glass”, a disordered state with extremely low entropy, or whether in principle a liquid may be supercooled to arbitrary low temperature. Among the challenges that lie in tackling the glass transition are the immense timescales involved. Computer simulation, which might otherwise be able to pick up hints of a thermodynamic transition, is limited by the small time-window over which a liquid can be equilibrated. Here we address this challenge using trajectory sampling in a system undergoing a first-order *non-equilibrium* phase transition to a glassy state rich in low-energy geometric motifs. Extrapolation indicates that this transition might become accessible in *equilibrium* at a temperature close to the so-called Kauzmann temperature. Furthermore, the low energy configurations representative of very low temperatures provide an illustration of the structural properties of glasses at extremely low configurational entropies.

I. INTRODUCTION

Although statistical mechanics has been firmly established more than hundred years ago [1], simple liquids remain a persistent challenge when cooled to low temperatures. In particular the dramatic super-Arrhenius increase of the relaxation time so far eludes a generally accepted explanation. A multitude of theoretical approaches has been advanced [2–4], but obtaining data that enables discrimination between these is challenging, due not least to the difficulties in handling the huge timescales required to equilibrate such supercooled liquids. At some point (typically bypassing crystallization) the relaxation time τ_α exceeds the experimentally or numerically accessible time scale t_{obs} and the liquid falls out of equilibrium into a dynamically arrested state called a glass.

The idea that a true phase transition is controlling dynamic arrest has been around for a long time, starting with an observation by Kauzmann [5]: extrapolating the configurational entropy of the liquid suggests that it should fall below that of the crystalline solid at a finite (Kauzmann) temperature T_K . One resolution of this apparent paradox is to posit a thermodynamic transition to an “ideal glass” with very low configurational entropy. More recent theories continue to use the language of phase transitions although they disagree on even the most basic assumptions. On one hand the emergence of criticality in a rugged free-energy landscape is anticipated through freezing, not to a single crystal but to a vast number of random, aperiodic states [6]; a picture that finds justification from mean-field results obtained in higher dimension [7, 8]. Approaches based on replica symmetry breaking also imagine a phase transition to state where configurations are closely related to one another, i.e. they have high overlap [9]. Another example,

geometric frustration, posits that geometric motifs that minimise the local free energy (locally favoured structures - LFS) are favoured upon supercooling and that the arrest seen is a manifestation of an avoided phase transition. Approaching the ideal glass transition, the system may seek to minimise its entropy, which can correspond to an increase in LFS [10].

Quite in contrast, in dynamical facilitation theory [4] dynamical correlations are the fundamental mechanism for the slow-down with static correlations being absent or at least irrelevant. Again the notion of a phase transition is pivotal, but now the transition is between two dynamic regimes: the supercooled liquid and a state with extremely slow dynamics [11]. The mathematical framework is that of statistical mechanics combined with large deviations [12]. The transition shares many similarities with the disorder-order transition of an Ising magnet; the main conceptual difference being that configurations are replaced by trajectories and the order parameter measures particle motion instead of magnetization. An intriguing prediction is the coexistence between the two dynamical regimes, which in lattice models is predicted to terminate in two critical points [13]. While numerical evidence supports coexistence and a first-order transition [11, 14], the putative lower critical point remains out of reach for direct numerical investigations in atomistic models.

Although structural changes appear to be minor when looking at two-point measures like the structure factor, the population of locally favoured structures and related structural motifs show a strong temperature-dependence [15]. Indeed, the dynamical transition to a liquid with very low particle mobility can be driven by increasing the LFS population [16], indicating that these structural changes are not only a byproduct of cooling but play a crucial role in the dynamic arrest. This finding is corroborated by simulations showing that single

particle motion and LFS are correlated [17].

Numerical simulations are an indispensable tool to gain microscopic insights. However, accessible time scales are still nine to ten decades away from the experimental glass transition temperature and more indirect methods have to be devised. For example, pinning (or confinement) of particles [18–20] shifts the putative thermodynamic transition into the time-window accessible to computer simulation, as has the observation of distributions of overlaps in configurations of particles [21]. A further method to generate deeply supercooled, equilibrated configurations is particle swaps [22, 23].

Here we tackle the challenge of determining the low-temperature equilibrium behavior of a popular atomistic glass former, the Kob-Andersen binary mixture [24], which is loosely based on the metallic glass former $\text{Ni}_{80}\text{P}_{20}$. To this end we introduce a powerful numerical method that exploits three effects: First, the central configurations of biased trajectories contain many LFS. Second, a higher population of LFS facilitates the sampling of configurations with low energies even at moderately supercooled temperatures. Adapting existing methods to remove the simulation bias, not only the simulated state point but a region in its vicinity becomes accessible. The third effect is that the contribution to the total free energy from the local minima in the potential energy landscape and from the vibrational free energy decouple [25]. This allows us to access equilibrium properties at configurational temperatures T (as opposed to the “vibrational” temperature) different from the sampling temperature T_s .

Using the described method, we perform extensive biased simulations for the Kob-Andersen mixture, from which we construct part of the phase diagram for the dynamic first-order transition from LFS-poor to LFS-rich. We find numerical evidence that coexistence is terminated at a finite temperature, which implies a lower critical point accessible by the equilibrium system—if it could be cooled sufficiently slowly. This scenario has significant consequences because the dynamical transition at a higher temperature thus probes the same glassy states while circumventing the prohibitive increase of equilibration times.

II. METHODS

A. Model

The Kob-Andersen binary mixture [24] consists of 80% large particles and 20% small particles interacting through truncated and shifted Lennard-Jones pair potentials. We employ the original potential parameters. All numerical values are reported in Lennard-Jones units with respect to the large particles, and we set Boltzmann’s constant to unity. Simulations are performed for a system of N particles at number density $N/V = 1.2$ in a periodic box with constant volume V . We em-

ploy the Andersen thermostat at sampling temperatures $T_s = 0.7, 0.6, 0.55, 0.5$. Newton’s equations of motion are solved using Verlet’s velocity algorithm with timestep 0.005 [26]. Trajectories are then stored as discrete sequences $X = \{\mathcal{C}_{-K/2}, \dots, \mathcal{C}_0, \dots, \mathcal{C}_{K/2}\}$ of configurations for lengths $K = 60$ and $K = 100$. The time between successive configurations is chosen such that trajectories have a physical duration of $t_{\text{obs}} \approx 4.5\tau_\alpha, 7.5\tau_\alpha$, respectively. Upon cooling the structural relaxation time increases faster than exponentially (super-Arrhenius behavior), see Fig. 1a. Whether the relaxation time diverges at a finite temperature is still debated [27, 28].

B. Order parameters

In the following we focus on two order parameters characterizing the liquid. The first, *dynamical* order parameter

$$\mathcal{N}[X] = \sum_{i=-K/2}^{K/2} n(\mathcal{C}_i) \quad (1)$$

characterizes trajectories by counting the total number of particles in LFS, where $n(\mathcal{C})$ is the fraction of particles in locally favoured structures in configuration \mathcal{C} . For the specific model considered here, the LFS corresponds to a bicapped square antiprism formed by 11 particles as sketched in the inset of Fig. 1a. We detect this motif employing the topological cluster classification method [29, 30]. The temperature dependence of the LFS population is fitted with the empirical Fermi function

$$\langle n \rangle = [1 + (T/T_{1/2})^\alpha]^{-1} \leq 1 \quad (2)$$

with fitted exponent $\alpha \simeq 2.5$ and temperature $T_{1/2} \simeq 0.25$ at which the population extrapolates to 1/2. The increase in LFS concentration (cf. Fig. 1a) has been shown to correlate well with the propensity of particle mobility on lowering the temperature [17].

Steepest descent quenches of the central configurations \mathcal{C}_0 to the local minima of the energy landscape yield the so-called inherent states [31], which may be thought of as particle configurations with the thermal noise removed. These inherent states $\mathcal{C}_0^{\text{is}}$ constitute the local minima in the energy landscape around which particles vibrate before reaching another local minimum. While in a perfect crystal there would be only one inherent state, in the liquid there are many different particle arrangements, and the number of these accessible amorphous inherent states defines the configurational entropy. Our second, *static* order parameter is thus the inherent state energy (ISE) per particle $\phi[X] = U(\mathcal{C}_0^{\text{is}})/N$ of the *central* configuration of trajectory X , where $U(\mathcal{C})$ is the potential energy of particle configuration \mathcal{C} and \mathcal{C}^{is} is the corresponding inherent state.

Practically, the ISE ϕ of central configurations \mathcal{C}_0 are obtained using the FIRE algorithm [32] limited to 1000

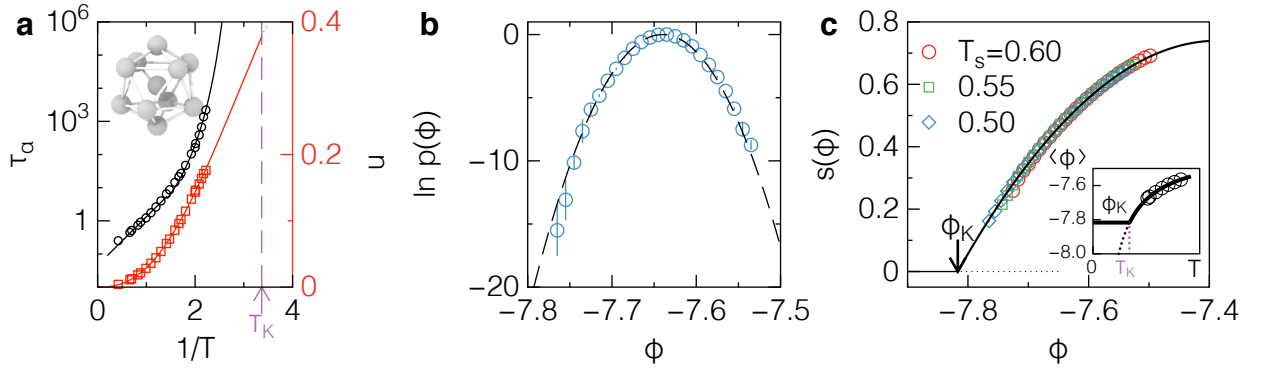


FIG. 1: Relaxation time and configurational entropy of the Kob-Andersen mixture. (a) The relaxation time (black circles) strongly increases as a function of inverse temperature. Also shown is the Vogel-Fulcher-Tamman expression $\ln \tau_\alpha \propto (T - T_K)^{-1}$ (solid line), which diverges at T_K (arrow). Along with the relaxation time the average population $\langle n \rangle$ of LFS (red squares, see inset for a rendering of the structure) increases upon cooling. The red line is an empirical two parameter fit to Eq. (2). (b) The probability distribution of the inherent state energy ϕ is Gaussian (dashed line, shown for sampling temperature $T_s = 0.5$). (c) Collapse of the configurational entropy $s(\phi)$ for three different sampling temperatures and fitted by a quadratic form (continuous line) down to very low energies. The energy $\phi_K \simeq -7.82$ at which the entropy would vanish is obtained from an extrapolation. In the inset, we use ϕ_K to estimate $T_K \approx 0.30$ by extrapolating molecular dynamics results (black circles).

iterations in order to make the generation of long sequences of trajectories computationally feasible. Ground states of equivalent energies have been obtained employing basin hopping techniques [33] confirming that the reported values for ϕ should be understood as upper (although tight) bounds to the true inherent state energies.

C. Biased simulations

We go beyond the temperature regime that is accessible in conventional molecular dynamics simulations. To this end biased simulations with $N = 216$ and $N = 400$ particles are run at a moderately supercooled sampling temperature T_s to faster explore phase space while at the same time sampling configurations with very low potential energy and a high population of LFS. To improve the sampling we employ replica exchange [14]. We simultaneously extract dynamic and static informations by harvesting trajectories of length t_{obs} , which we choose to be a few structural relaxation times $t_{\text{obs}} \approx 4.5\tau_\alpha$ and $t_{\text{obs}} \approx 7.5\tau_\alpha$ for runs with $K = 60$ and $K = 100$ configurations, respectively.

We employ the multistate Bennet acceptance ratio (MBAR) estimator [34, 35] in order to calculate expectations and distributions from the biased numerical data. For an arbitrary observable $A[X]$, this amounts to evaluating the expression

$$\langle A \rangle_{T,\mu} = \frac{\langle A e^{-\beta N \phi + \mu \mathcal{N}} \rangle}{\langle e^{-\beta N \phi + \mu \mathcal{N}} \rangle}, \quad (3)$$

where $\langle \cdot \rangle$ indicates the average over the sampled trajectories at sampling temperature T_s . Here, $\beta = 1/T - 1/T_s$ with T denoting the target configurational temperature and μ the dynamical chemical potential.

In practice, our numerical approach allows us to improve the sampling of trajectories that are rare for a given sampling temperature T_s , explicitly favoring trajectories with exceptionally large (or small) overall concentrations of LFS n through performing importance sampling in trajectory space. Transition path sampling [36] is performed according to the structural bias in n but any observable (including both ϕ and n) can be simultaneously tracked and its correct probability distribution, and in particular its mean value, can be recovered reassigning the correct weight to each trajectory, as illustrated by Eq. 3.

D. Temperature reweighting

The harvested trajectories also yield equilibrium expectation values beyond the sampling temperature for observables $A[X] = A(\mathcal{C}^{\text{is}})$ that depend on inherent state configurations \mathcal{C}^{is} only; provided that (i) configurations are sampled according to the Boltzmann weight $\propto e^{-U(\mathcal{C})/T_s}$ (at the sampling temperature), and (ii) vibrations are independent of the inherent state. Now, previous work [25] has demonstrated via thermodynamic integration that for sufficiently low temperatures ($T < 0.8$), the contribution of the inherent state energies to the free energy decouples from the vibrational contribution.

To show how it is possible to extract the equilibrium statistics of inherent state energies from the trajectory sampling, we split the total potential energy

$U(\mathcal{C}) = N\phi(\mathcal{C}^{\text{is}}) + \delta U(\mathcal{C}|\mathcal{C}^{\text{is}})$, leading to

$$\begin{aligned} \langle Ae^{-\beta N\phi} \rangle &= \sum_{\mathcal{C}^{\text{is}}} \sum_{\mathcal{C}|\mathcal{C}^{\text{is}}} A(\mathcal{C}^{\text{is}}) e^{-\beta N\phi} \frac{1}{Z(T_s)} e^{-(N\phi + \delta U)/T_s} \\ &= \frac{1}{Z(T_s)} \sum_{\mathcal{C}^{\text{is}}} A(\mathcal{C}^{\text{is}}) e^{-N\phi(\mathcal{C}^{\text{is}})/T} \tilde{Z}(T_s|\mathcal{C}^{\text{is}}) \end{aligned}$$

with partition sum $Z(T) = \sum_{\mathcal{C}} e^{-U(\mathcal{C})/T}$ and restricted partition sum $\tilde{Z}(T|\mathcal{C}^{\text{is}})$ sampling the fluctuations out of the inherent state \mathcal{C}^{is} . If the restricted partition sum is approximately independent of the inherent state, $\tilde{Z}(T|\mathcal{C}^{\text{is}}) \approx \tilde{Z}(T)$, we obtain

$$\langle A \rangle_{T,\mu=0} = \frac{\sum_{\mathcal{C}^{\text{is}}} Ae^{-N\phi/T}}{\sum_{\mathcal{C}^{\text{is}}} e^{-N\phi/T}} \quad (4)$$

corresponding to the equilibrium expectation of A at temperatures $T \neq T_s$ different from the sampling temperature.

III. RESULTS

A. Configurational entropy

We first focus on the behavior of the central configurations. Our simulations sample configurations with a wide range of ISE, which we compile into distributions $p(\phi)$ for the different sampling temperatures. In agreement with previous studies [25, 37], we find that these distributions are well described by a Gaussian, see Fig. 1b. Moreover, it has been demonstrated that at low enough temperature (including the sampling temperature $0.5 \leq T_s \leq 0.7$ used here) the vibrational free energy is independent of ϕ to a very good approximation [25].

Let $\Omega(\phi) \propto \Omega_{\infty} e^{N\sigma(\phi)} \delta\phi$ be the number of *amorphous* inherent states with energy per particle ϕ within an interval $\phi \pm \delta\phi/2$. Here, $\sigma(\phi)$ is the enumeration function and $\Omega_{\infty} \simeq e^{Ns_{\infty}}$ is the maximal available volume in configuration space. The (configurational) temperature T corresponds to the inverse slope, $d\sigma/d\phi = 1/T$. In the limit of large N , the number Ω is either extensive or becomes exponentially small. Hence, in the thermodynamic limit, the extensive configurational entropy becomes $\ln \Omega(\phi) \simeq Ns(\phi)$ with $s(\phi) = s_{\infty} + \sigma(\phi)$ for $\phi \geq \phi_K$ and $s(\phi) = 0$ for extreme energies $\phi < \phi_K$.

We extract the quadratic enumeration function $\sigma(\phi) = -(\phi - \phi_{\infty})^2/J^2$ from the measured distribution with fitted maximal energy $\phi_{\infty} \simeq -7.38$ and scale $J \simeq 0.502$. The resulting configurational entropy $s(\phi) = s_{\infty} + \sigma(\phi)$ is plotted in Fig. 1c using the value $s_{\infty} \simeq 0.74$ reported previously [25]. Our numerical scheme is thus able to cover a wide range of inherent states and the excellent agreement demonstrates that the configurational entropy of the liquid is indeed very well described by a quadratic function.

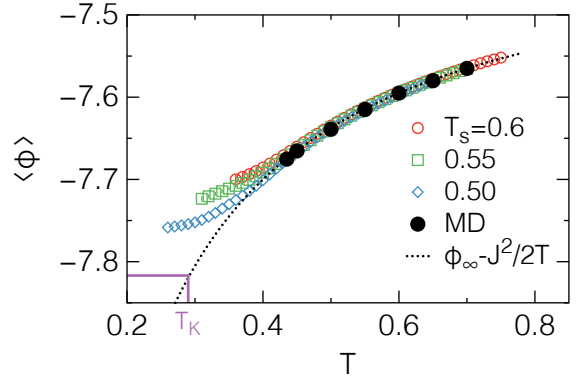


FIG. 2: Importance sampling of inherent state energies at sampling temperatures $T_s = 0.60, 0.55, 0.50$. The dotted line indicates the prediction of Eq. 5 for the equilibrium liquid, while filled symbols represent the values obtained from unbiased Molecular Dynamics simulations. Deviations from the equilibrium liquid occur only at low T and become smaller if the sampling is performed at lower T_s . Also indicated is the putative value of the Kauzmann temperature T_K and the corresponding energy of the equilibrium liquid.

For the thermal average one finds

$$\langle \phi \rangle = \phi_{\infty} - \frac{J^2}{2T} \quad (5)$$

as a function of temperature T . The scenario that $\langle \phi \rangle = \phi_K$ with $\phi_K \simeq -7.82$ is reached at a finite temperature T_K is shown in Fig. 1c by extrapolating simulation data. Figuratively speaking, at this temperature the liquid would “run out” of amorphous configurations and would undergo a thermodynamic phase transition to an ideal glass with constant inherent state energy ϕ_K and very low entropy. Although the existence of such an ideal glass state is debated on several grounds, e.g. [38, 39], we keep ϕ_K as a convenient estimate for the lowest energy accessible to amorphous configurations. Extrapolating the quadratic form for $s(\phi)$ to lower energies, one derives $T_K = J/(2\sqrt{s_{\infty}})$ for the Kauzmann temperature yielding $T_K \simeq 0.30$ for the present system in agreement with a previous estimate [25]. This value is compatible with an extrapolation of molecular dynamics data for the average ISE $\langle \phi \rangle$, which we show in the inset of Fig. 1c. Comparing with the increase of τ_{α} (Fig. 1a), it is clear that T_K is far below temperatures for which the liquid can be equilibrated in computer simulations.

In Fig. 2 the average ISE $\langle \phi \rangle_{T,\mu=0}$ is shown as a function of (configurational) temperature T employing the described scheme, showing good agreement with data obtained from molecular dynamics simulations. Assuming that the Kauzmann energy ϕ_K represents the “bottom” of the energy landscape of amorphous states, then we expect that for $T < T_K$ there should be no further reduction in $\langle \phi \rangle$, which is indeed supported by our data for successively lower sampling temperatures T_s .

B. Dynamical phase transition from LFS-poor to LFS-rich

We now consider the full trajectories. Formally, one can treat the particles in LFS and free particles as two chemical species with the same chemical potential that interconvert freely. The extension to ensembles of trajectories is, at least formally, straightforward with μ the dynamical analogon of the chemical potential difference. Unbiased equilibrium dynamics still corresponds to $\mu = 0$. In line with physical intuition, positive $\mu > 0$ gives trajectories with larger population a higher weight, which is demonstrated in Fig. 3a. Here we show the average population $\langle n \rangle_{T_s, \mu}$ of LFS as a function of μ for the three sampling temperatures. At some $\mu_* > 0$ there is a sharp increase of the population indicating a transition from the normal supercooled liquid (LFS-poor) to a state composed of trajectories comprising a large number of LFS (LFS-rich). Indeed, it has been shown that the transition becomes sharper for larger systems [16], where “larger” can be both larger t_{obs} (longer trajectories) and larger N (more particles while holding the density constant). This implies a first-order transition in trajectory space, where the jump of the order parameter (the population of LFS) is rounded by finite-size effects [40]. Practically, the value of μ_* is determined from the peak of the susceptibility

$$\chi(\mu) = \frac{\partial \langle n \rangle_{T_s, \mu}}{\partial \mu} \quad (6)$$

maximizing the fluctuations of the order parameter. The susceptibility measures the sensitivity of the population when changing the field. It becomes very large close to the phase transition and is expected to diverge in the limit of infinite system size. Note that decreasing the sampling temperature, the peak position moves towards $\mu = 0$, which corresponds to the unbiased, equilibrium dynamics. We return to the intriguing question of the low temperature behavior of μ_* below. Moreover, the peak height $\chi_* = \chi(\mu_*)$ grows.

Having identified an LFS-poor and an LFS-rich phase, in Fig. 3a we show that the transition is accompanied by a complementary drop of the inherent state energies of central configurations [41]. Indeed, looking at the joint distribution of n and ϕ in Fig. 3b, two distinct populations of trajectories can be discerned. In particular, trajectories with a large number of LFS comprise central configurations that typically have low inherent state energy. From the marginal distribution of ISE (inset of Fig. 3c) we extract the two typical values ϕ_{poor} and ϕ_{rich} for LFS-poor and LFS-rich states, respectively, as a function of configurational temperature T , using Eq. 3. These we plot in Fig. 3(c). The inherent state energies for the normal, LFS-poor liquid follow the prediction of Eq. (5) for the average ISE. In contrast, the much lower ϕ_{rich} shows a more complex behaviour: at high temperatures, the different T_s converge at the same energy, which is a slow monotonically increasing function of the configura-

tional temperature T . For the lowest temperatures T , there is a systematic dependence on the sampling temperature T_s , with lower T_s allowing to better sample lower energy states and thus leading to lower average ISE. Due to the much weaker dependence on T of ϕ_{rich} , the energy gap $\phi_{\text{poor}} - \phi_{\text{rich}}$ is reduced with decreasing T , so that it suggests the existence of a finite temperature T_* at which the two energies reach the same value and the gap vanishes.

C. Non-equilibrium phase diagram

To construct the phase diagram we determine the populations n_{poor} and n_{rich} of the coexisting LFS-poor and LFS-rich states, respectively. To this end we produce histograms of the LFS population at $\mu = \mu_*$ and determine the positions of the two peaks corresponding to either phase (see Fig. 4a inset). These populations delimit the coexistence region as shown in Fig. 4a for several sampling temperatures. They agree within errors for different trajectory lengths and system sizes ($N = 216$ and $N = 400$ particles). The unbiased equilibrium dynamics with $\mu = 0$ corresponds to a line in the (T, n) plane as shown in red in Fig. 4a, any point away from this line corresponds to a non-equilibrium state with $\mu \neq 0$. For the temperatures that we can sample directly the equilibrium LFS population lies within the LFS-poor region but remarkably close to coexistence.

IV. DISCUSSION

A. A lower critical point?

The existence of a genuine thermodynamic phase transition for glass forming fluids is widely debated [2–4, 38]. In the case of the Kob-Andersen mixture, there are several pieces of numerical evidence pointing towards a transition at temperatures substantially below the avoided Mode-Coupling transition temperature $T_{\text{MC}} \simeq 0.435$: (i) Thermodynamic integration [25] provides, through an extrapolation, an estimate for a finite Kauzmann temperature T_K at which the configurational entropy vanishes. (ii) As previously mentioned, relaxation times can be thought to diverge in the vicinity of T_K , providing a dynamical description of the transition (see Fig. 1a). (iii) Recent equilibrium simulations [19] in presence of a variable concentration of pinned particles c show that in the limit of vanishing $c \rightarrow 0$ a transition between a more and a less “glassy” thermodynamic state (as indicated by the so-called overlap order parameter, see [19] and references therein) can be inferred at a nonzero temperature close to T_K . (iv) Finally, the same overlap order parameter [42] has been used to show that static fluctuations exist for $T \lesssim 0.5$, consistent with the existence of a random critical point predicted by effective field theories [43, 44].

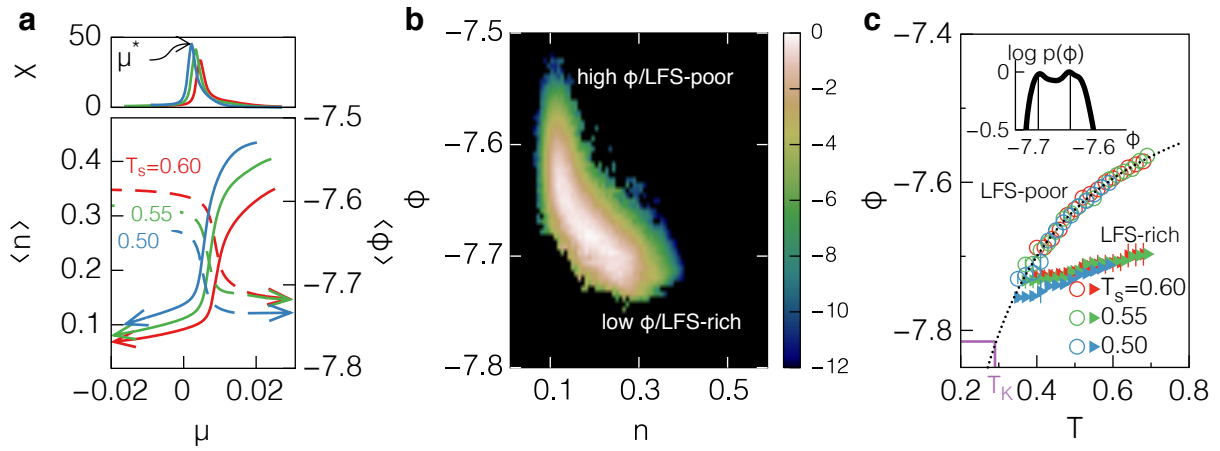


FIG. 3: The inherent state energy drops across the dynamical transition. (a) Signature of the dynamical phase transition: the average trajectory population $\langle n \rangle_{T_s, \mu}$ of LFS (continuous lines) shows a sudden increase at a non-zero μ . Top, the susceptibility $\chi(\mu)$ quantifying the magnitude of fluctuations is shown, the peak of which defines μ_* . Around the same μ_* , the average ISE $\langle \phi \rangle_{T_s, \mu}$ of central configurations (dashed lines) drops substantially. (b) Logarithm of the joint probability of LFS population n and ISE ϕ , for $T_s = 0.55$ and $\mu = 0.005 \approx 0.7\mu_*$. (c) Typical energies of the two populations as a function of temperature: LFS-poor states (circles) essentially follow the equilibrium fluid curve (dotted line) while LFS-rich ones (filled triangles) are characterised by much lower energies, with a T_s -dependent tail at low temperatures. Inset: ISE probability distribution $p(\phi)$ evaluated at $\mu = \mu_*$ for $T = 0.55$.

In our case, the thermodynamic behaviour of the system follows from the more general and complex description of its non-equilibrium phase diagram, where the equilibrium limit corresponds to $\mu \rightarrow 0$. We find strong numerical evidence for a coexistence region between LFS-rich and LFS-poor trajectories, at least in the temperature interval $0.5 \leq T_s \leq 0.7$ directly probed by the biased simulations. The temperatures at which the distinction between LFS-rich and LFS-poor trajectories ceases would identify an upper and a lower critical point, the locations of which can only be inferred by extrapolation. In particular, the precise location of the lower critical point with respect to the equilibrium line would allow for a connection between the putative thermodynamic transition at T_K and the dynamical phase transition determined in the present work. In the following, we discuss our evidence for a thermodynamic transition and also discuss alternative scenarios.

B. Numerical evidence

To interpret our numerical results, we first consider the population of LFS at coexistence, $n_*(T) = \langle n \rangle_{T, \mu_*}$. As shown in Fig. 4a (green line), the dependence of n_* on temperature is linear to a very good degree. Extrapolating towards lower temperatures, it crosses the equilibrium ($\mu = 0$) line with $n_*(T_0) = \langle n \rangle_{T_0, \mu=0}$, which implies $n_{\text{poor}} = n_{\text{rich}}$. The crossing of both lines occurs at a temperature $T_0 \simeq 0.29$ close to the estimated value for the Kauzmann temperature T_K .

Our second piece of evidence comes from the extrapolation of the dynamical chemical potential μ_* at coexistence. In Fig. 4b the phase diagram has been recast into the $T - \mu$ plane, with the coexistence region being reduced to a line separating the LFS-poor from the LFS-rich trajectories. Here we have plotted the different values of μ_* scaled with the trajectory length t_{obs} and observe that they collapse onto a common master curve. Down to the coldest sampling temperature $T_s = 0.50$, $\mu_*(T)$ follows a linear behaviour, the extrapolation of which to $\mu_* = 0$ provides a second estimate for a finite transition temperature $T_0 \simeq 0.33$ again close to the estimate $T_K \simeq 0.30$ for the Kauzmann temperature.

Finally, we note that the ISE of the LFS-rich configurations in Fig. 3c is approximately linear, $\phi_{\text{rich}}(T) = \phi_0 + \gamma T$, with fitted $\phi_0 \simeq -7.82$ (note that $\phi_0 \approx \phi_K$) and $\gamma \simeq 0.18$ for the lowest sampling temperature. Assuming that the vibrational free energy and the inherent states still decouple, for any transition the configurational temperatures (*i.e.*, the slopes of the configurational entropies of LFS-rich and LFS-poor phase) have to agree. For a putative continuous transition we equate the ISE and find $\phi \simeq -7.76$ with corresponding temperature $T_0 \simeq 0.33$, which agrees with the other two estimates.

C. The fate of the supercooled liquid

Although relying on extrapolations, these three pieces of numerical evidence indicate that the dynamical transition from LFS-poor to LFS-rich might become accessible for the unbiased supercooled liquid provided that it is cooled sufficiently slowly and crystallization does not in-

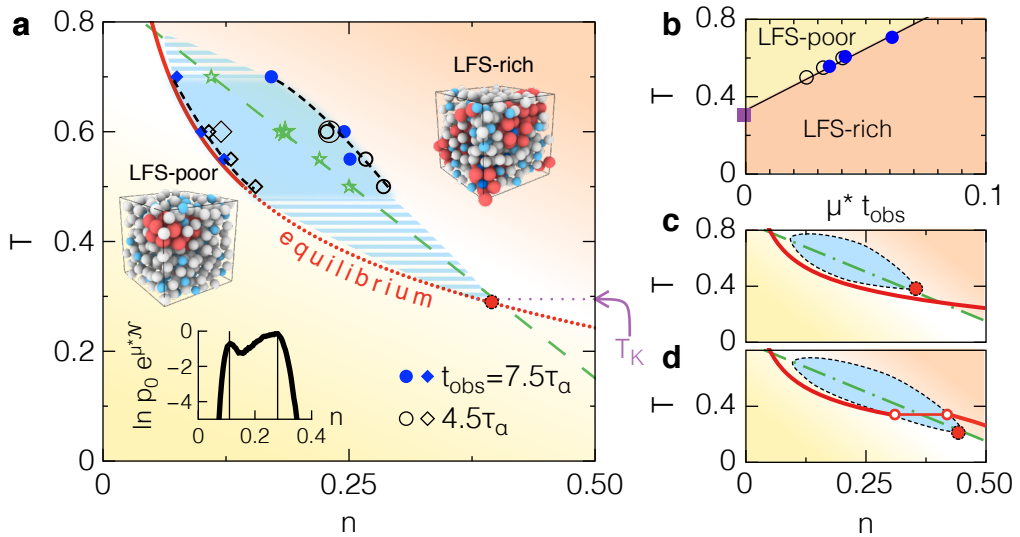


FIG. 4: Phase diagram and possible scenarios for a lower critical point. (a) Coexisting populations for $N = 216$ particles and several sampling temperatures (filled symbols $t_{\text{obs}} \approx 7.5\tau_{\alpha}$, empty symbols $t_{\text{obs}} \approx 4.5\tau_{\alpha}$) and $N = 400$ at $T_s = 0.6$ (larger empty symbols). Green stars denote $n_*(T) = \langle n \rangle_{T, \mu_*}$, fitted to a linear function (dashed-dotted green line). Based on these values a possible coexistence region is sketched (shaded area). The unbiased equilibrium dynamics (red continuous line, Eq. 2) passes through the supercooled, LFS-poor liquid. Shown is the scenario of a lower critical point of the dynamical transition passed by the unbiased dynamics. Two snapshots of LFS-rich and LFS-poor configurations are also illustrated, with the non-LFS particles in white. Inset: Example for the determination of the coexisting LFS populations from the peak positions of histograms $p(n)$ evaluated at $\mu = \mu_*$ for $T_s = 0.60$ and $t_{\text{obs}} = 4.5\tau_{\alpha}$. (b) Coexistence in the $T - \mu$ phase diagram, with μ_* scaled by the trajectory length. A linear fit leads to the estimate of the unbiased dynamics transition temperature $T_0 \approx T_K$ (purple square). Finally, (c) and (d) are sketches for two alternative scenarios: (c) an “avoided” transition and (d) a weakly first order transition.

terfere. From the numerical data we can bound the temperature at which this occurs by $T_K \leq T_0 < 0.33$. We speculate that a lower critical point exists at temperature T_* , terminating coexistence between LFS-poor and LFS-rich trajectories. This leads to three possible scenarios: First, the critical temperature $T_* > T_0$ is higher, in which case no equilibrium transition occurs but is passed closely (an avoided transition). At T_0 the unbiased dynamics then crosses the line emanating from the critical point where the fluctuations are maximal (sometimes called the “Widom line” [45, 46]), see Fig. 4c, analogously to some scenarios in softened kinetically constrained models [47]. Second, for $T_* = T_0$ the unbiased dynamics crosses through the critical point and a continuous transition occurs as depicted in Fig. 4a. Third, for $T_* < T_0$ the equilibrium transition would be (weakly) first order, as sketched in Fig. 4d.

V. CONCLUSIONS

By means of numerical simulations employing trajectory sampling, we have explored the connection between a dynamical phase transition and the low temperature thermodynamics of a well studied atomistic glass former. We have demonstrated that the identification of a locally favored structure and its use as an order parameter to bias the simulations at a given sampling temperature is

a powerful and reliable method to obtain equilibrium, thermodynamic information (such as the inherent state energies and the configurational entropy) down to very low temperatures. This is because trajectory sampling facilitates the exploration of states that are exponentially unlikely to be accessed in a conventional molecular dynamics simulation.

Employing the obtained probability distributions, we show that the dynamical phase transition in trajectory space implies a bimodal distribution of inherent state energies: For the equilibrium dynamics most of the configurations are compatible with a high energy, LFS-poor state. However, we also reveal that an amorphous, locally favoured structure-rich, low energy state exists and is accessible when the dynamical chemical potential μ is tuned away from zero [16]. Employing our numerical technique, we also determine the temperature dependence of the energy gap between the two states, which provides numerical evidence for a lower critical point at a non-zero temperature T_0 where the LFS-poor phase would be indistinguishable from the LFS-rich phase. This is further corroborated by the temperature at which the first order dynamical phase transition appears to cross the unbiased dynamics ($\mu \rightarrow 0$). Numerically, we find that the temperature T_0 is close to the estimated Kauzmann temperature.

Our results support the idea that the low temperature fate of supercooled atomistic glass formers is de-

terminated by the fluctuations of the population of local structures. There is now ample numerical evidence that particle dynamics, at least for a class of strongly non-mean-field model glassformers [15, 17, 29], is correlated with the presence of LFS. We attribute the emergence of slow dynamics, dynamical heterogeneities, and critical-like behaviour to a (dynamical) critical point that terminates non-equilibrium coexistence of two structural phases, LFS-poor and LFS-rich. This opens a potential avenue to unify the competing theories that have been developed in order to understand the microscopic origin of slow glassy dynamics. Following this avenue for other model glass formers with different fragilities and different structural signatures [17], and comparing it with existing theories for critical behaviour in glasses [43, 48] will be the challenging subject of future investigations.

Acknowledgments

The authors are grateful to Ludovic Berthier, Juan P. Garrahan, Robert L. Jack, Walter Kob and John Russo for helpful comments. Stephen Williams is gratefully acknowledged for helpful discussions and preliminary results. CPR acknowledges the Royal Society for funding and Kyoto University SPIRITS fund. FT and CPR acknowledge the European Research Council (ERC consolidator grant NANOPRS, project number 617266). This work was carried out using the computational facilities of the Advanced Computing Research Centre, University of Bristol.

[1] J. Gibbs, *Elementary Principles in Statistical Mechanics* (C. Scribner's sons, 1902).

[2] A. Cavagna, Phys. Rep. **476**, 51 (2009).

[3] L. Berthier and G. Biroli, Rev. Mod. Phys. **83**, 587 (2011).

[4] D. Chandler and J. P. Garrahan, Annu. Rev. Condens. Matt. Phys. **61**, 191 (2010).

[5] W. Kauzmann, Chem. Rev. **43**, 219 (1948).

[6] T. R. Kirkpatrick, D. Thirumalai, and P. G. Wolynes, Phys. Rev. A **40**, 1045 (1989).

[7] V. Lubchenko and P. Wolynes, Ann. Rev. Phys. Chem. **58**, 235266 (2007).

[8] P. Charbonneau, J. Kurchan, G. Parisi, P. Urbani, and F. Zamponi, Nat. Commun. **5**, 3725 (2014).

[9] G. Parisi and F. Zamponi, Reviews of Modern Physics **82**, 789 (2010).

[10] G. Tarjus, S. A. Kivelson, Z. Nussinov, and P. Viot, J. Phys.: Condens. Matter **17**, R1143 (2005).

[11] L. O. Hedges, R. L. Jack, J. P. Garrahan, and D. Chandler, Science **323**, 1309 (2009).

[12] H. Touchette, Phys. Rep. **478**, 1 (2009).

[13] Y. S. Elmatad, R. L. Jack, D. Chandler, and J. P. Garrahan, Proc. Nat. Acad. Sci. **107**, 12793 (2010).

[14] T. Speck and D. Chandler, J. Chem. Phys. **136**, 184509 (2012).

[15] D. Coslovich and G. Pastore, J. Chem. Phys. **127**, 124504 (2007).

[16] T. Speck, A. Malins, and C. P. Royall, Phys. Rev. Lett. **109**, 195703 (2012).

[17] G. M. Hocky, D. Coslovich, A. Ikeda, and D. Reichman, Phys. Rev. Lett. **113**, 157801 (2014).

[18] C. Cammarota, A. Cavagna, I. Giardina, G. Gradenigo, T. S. Grigera, G. Parisi, and P. Verrocchio, Phys. Rev. Lett. **105**, 055703 (2010).

[19] M. Ozawa, W. Kob, A. Ikeda, and K. Miyazaki, Proceedings of the National Academy of Sciences **112**, 6914 (2015).

[20] D. A. Martín, A. Cavagna, and T. S. Grigera, Phys. Rev. Lett. **114**, 225901 (2015).

[21] L. Berthier, Phys. Rev. E **88**, 022313 (2013).

[22] S. Gutiérrez, R. Karmakar, Y. G. Pollack, and I. Procaccia (2014), arXiv:1409.5067.

[23] L. Berthier, D. Coslovich, A. Ninarello, and M. Ozawa (2015), arXiv:1511.06182.

[24] W. Kob and H. C. Andersen, Phys. Rev. Lett. **73**, 1376 (1994).

[25] F. Sciortino, W. Kob, and P. Tartaglia, Phys. Rev. Lett. **83**, 3214 (1999).

[26] S. Plimpton, J. Comput. Phys. **117**, 1 (1995).

[27] T. Heckscher, A. I. Nielsen, N. B. Olsen, and J. C. Dyre, Nature Phys. **4**, 737 (2008).

[28] Y. S. Elmatad, D. Chandler, and J. P. Garrahan, J. Phys. Chem. B **114**, 1711317119 (2010).

[29] A. Malins, J. Eggers, H. Tanaka, and C. P. Royall, Faraday Discuss. **167**, 405 (2013).

[30] A. Malins, S. R. Williams, J. Eggers, and C. P. Royall, J. Chem. Phys. **139**, 234506 (2013).

[31] T. A. Weber and F. H. Stillinger, Phys. Rev. B **31**, 1954 (1985).

[32] E. Bitzek, P. Koskinen, F. Gähler, M. Moseler, and P. Gumbsch, Phys. Rev. Lett. **97**, 170201 (2006).

[33] D. J. Wales and J. P. Doye, J. Phys. Chem. A **101**, 5111 (1997).

[34] M. R. Shirts and J. D. Chodera, J. Chem. Phys. **129**, 124105 (2008).

[35] D. D. L. Minh and J. D. Chodera, J. Chem. Phys. **131**, 134110 (2009).

[36] C. Dellago, P. G. Bolhuis, and P. L. Geissler, Adv. Chem. Phys. **123**, 1 (2002).

[37] S. Büchner and A. Heuer, Phys. Rev. E **60**, 6507 (1999).

[38] F. H. Stillinger, J. Chem. Phys. **88**, 7818 (1988).

[39] A. Donev, F. H. Stillinger, and S. Torquato, J. Chem. Phys. **127**, 124509 (2007).

[40] M. S. S. Challa, D. P. Landau, and K. Binder, Phys. Rev. B **34**, 1841 (1986).

[41] R. L. Jack, L. O. Hedges, J. P. Garrahan, and D. Chandler, Phys. Rev. Lett. **107**, 275702 (2011).

[42] L. Berthier and R. L. Jack, Phys. Rev. Lett. **114**, 205701 (2015).

[43] S. Franz and G. Parisi, J. Stat. Mech. **2013**, P11012 (2013).

[44] G. Biroli, C. Cammarota, G. Tarjus, and M. Tarzia, Phys. Rev. Lett. **112**, 175701 (2014).

[45] B. Widom, J. Chem. Phys. **43**, 3898 (1965).

- [46] L. Xu, P. Kumar, S. V. Buldyrev, S.-H. Chen, P. H. Poole, F. Sciortino, and H. E. Stanley, Proc. Nat. Acad. Sci. **102**, 16558 (2005).
- [47] Y. S. Elmatad and R. L. Jack, J. Chem. Phys. **138**, 12A531 (2013).
- [48] S. K. Nandi, G. Biroli, J.-P. Bouchaud, K. Miyazaki, and D. R. Reichman, Phys. Rev. Lett. **113**, 245701 (2014).